Journal of Hydrology 610 (2022) 127964

Contents lists available at ScienceDirect

Journal of Hydrology

journal homepage: www.elsevier.com/locate/jhydrol

Research papers

Characterizing the spatiotemporal dynamics of shallow soil water stable isotopic compositions on a karst hillslope in Southwestern China

Qin Liu [a], Tiejun Wang [a,b,c,*], Cong-qiang Liu [a,b,c], Espoire M.R.B. Mikouendanandi [a], Xi Chen [a,b,c], Tao Peng [d,e], Lin Zhang [d]

[a] Institute of Surface-Earth System Science, School of Earth System Science, Tianjin University, Weijin Road 92, Tianjin 300072, China
[b] Critical Zone Observatory of Bohai Coastal Region, Tianjin University, Tianjin 300072, China
[c] Tianjin Key Laboratory of Earth Critical Zone Science and Sustainable Development in Bohai Rim, Tianjin University, Weijin Road 92, Tianjin 300072, China
[d] Puding Karst Ecosystem Research Station, Chinese Ecosystem Research Network, Chinese Academy of Sciences, Puding 562100, Guizhou, China
[e] Institute of Geochemistry Chinese Academy of Sciences, Guiyang 550081, China

ARTICLE INFO

Keywords:
Soil water stable isotopic composition
Shallow soil water
Spatiotemporal dynamics
Temporal stability
Karst

ABSTRACT

Knowledge of the spatiotemporal dynamics of soil water content (SWC) and soil water stable isotopic compositions (SWSIC) is critical for understanding water exchanges across the atmosphere-land interface. However, compared with those of SWC, studies on the spatiotemporal characteristics of SWSIC are still scarce, which limits their use for more accurately characterizing terrestrial ecohydrological processes. To examine whether SWSIC and SWC share similar spatiotemporal features, their spatiotemporal patterns along with relevant controls were investigated at shallow soils (0–10 cm) on a karst hillslope in Southwest China, based on seven sampling campaigns conducted over a two-year period. The results revealed considerable spatiotemporal variations in SWSIC. Compared to SWC, δD values exhibited smaller spatial variations, while line-conditioned excess (lc-excess) values exhibited considerably larger ones, suggesting that soil evaporation heterogeneity might not be the primary reason for spatial variations in δD of soil water in this study. The spatial structures of SWSIC were less temporally stable than those of SWC due to the combined impact of land surface processes and temporal variations in isotopic compositions of input water on SWSIC. Moreover, the spatiotemporal patterns of SWSIC were less explained by environmental variables that were also differed from those of SWC, suggesting that the knowledge gained from SWC studies might not be directly transferable to understand SWSIC spatiotemporal characteristics. Nevertheless, it should be highlighted that the temporal stability analysis method initially proposed for studying SWC could be extended to select representative sites for monitoring areal average SWSIC, due to the temporal persistence of the SWSIC spatial structures. In addition, a negative correlation between the spatial mean and standard deviation of lc-excess was found, indicating that the associated spatial variability increased with areal mean kinetic fractionation signals caused by soil evaporation. These findings have important implications for designing SWSIC monitoring schemes, which in turn can improve the interpretation of SWSIC data for various application purposes.

1. Introduction

As a key component in land surface systems, soil water has significant impacts on water, energy, and biogeochemical exchanges across the atmosphere-land interface (Seneviratne et al., 2010; Liu et al., 2019; Wu et al., 2021). To characterize soil water dynamics and trace soil water movements, soil water content (SWC) and soil water stable isotopic compositions (SWSIC; e.g., δD and $\delta^{18}O$) are routinely used (Vereecken et al., 2008; Sprenger et al., 2016). Compared to SWC as a state variable for depicting soil water dynamics, SWSIC can serve as ideal natural tracers for tracking water movements in the soil–plant-atmosphere continuum, e.g., illuminating water flow paths (Gazis and Feng, 2004; Xiang et al., 2019), quantifying soil water residence time (Chen et al., 2017; Sprenger et al., 2019), and elucidating soil evaporation processes (Sprenger et al., 2017a; Kleine et al., 2020). However, owing to the highly dynamic interactions between soil water and environmental variables (e.g., soil compositions, topography, and vegetation), there still exist large gaps in applying SWC and SWSIC for revealing related

* Corresponding author at: Institute of Surface-Earth System Science, School of Earth System Science, Tianjin University, Tianjin 300072, China.
E-mail address: tiejun.wang@tju.edu.cn (T. Wang).

https://doi.org/10.1016/j.jhydrol.2022.127964
Received 22 November 2021; Received in revised form 9 April 2022; Accepted 20 May 2022
Available online 25 May 2022

hydrological and ecohydrological processes (Vereecken et al., 2008; Sprenger et al., 2016).

Appropriately interpreting SWC and SWSIC data is challenging due to the uncertainties associated with the spatiotemporal variations in hydrological and ecohydrological processes (Troch et al., 2009; Beyer and Penna, 2021). To improve the accuracy of SWC-based estimations, extensive efforts have been devoted to understanding SWC spatiotemporal patterns across scales and more importantly to elucidating the factors and processes that drive SWC spatiotemporal patterns (see the reviews by Seneviratne et al. (2010) and Vereecken et al. (2014)). Recent studies show that neglecting SWSIC heterogeneity could lead to biased or incorrect interpretations of SWSIC data for various application purposes (Penna and van Meerveld, 2019; Barbeta et al., 2020; Beyer and Penna, 2021). For example, Penna and van Meerveld (2019) showed that the estimated maximum contributions of different hydrological compartments (throughfall, soil water, and shallow groundwater) differed by up to 26% from the reference scenario when the spatial variability in isotopic composition of these three end-members was considered in hydrograph separations for a small catchment in Italy. Despite the potential importance of spatial variations in SWSIC, most SWSIC-related studies have focused on investigating soil water transport processes at the level of soil patches, with rare consideration given to the representativeness of these patches for larger areas (e.g., Evaristo et al., 2015; Sprenger et al., 2017b). The lack of data quantifying SWSIC spatiotemporal variations makes it difficult to evaluate the associated uncertainties when small-scale studies are used to understand large-scale ecohydrological processes (Penna et al., 2018).

In spite of the scarcity of data quantifying SWSIC variations, some field studies have revealed large spatial variability in SWSIC (Thomas et al., 2013; Oshun et al., 2016; Yang et al., 2016; Goldsmith et al., 2018a; Oerter and Bowen, 2019; Xu et al., 2022). For instance, based on one campaign of 150 points, Goldsmith et al. (2018a) observed considerable spatial variations in δD (−83.4‰ ~ −33.2‰) and $\delta^{18}O$ values (−11.0‰ ~ −0.3‰) of shallow soil water at a humid forest in Switzerland, and showed that such variations were poorly explained by soil properties and often not predictable from measurements made at nearby points. With two campaigns of 130 points on a karst hillslope in Southwestern China, Yang et al. (2016) also showed huge spatiotemporal variations in δD values of shallow soil water (−69.1‰ ~ −20.5‰ in April and −50.2‰ ~ −81.1‰ in August). However, most studies of this kind have relied on very few sampling campaigns, making it challenging to capture the temporal characteristics of SWSIC spatial structures. Such facts thus hindered the applications of spatial variation information in illuminating ecohydrological processes under constantly changing environmental conditions. Therefore, more comprehensive studies about SWSIC spatiotemporal patterns are needed, which is critical for designing appropriate field sampling strategies.

Given that SWSIC variations caused by ecohydrological processes (such as mixing with pre-event soil water (Demand et al., 2019; Xiang et al., 2019), hydraulic redistribution (Rothfuss and Javaux, 2017), and soil evaporation (Quade et al., 2018)) are often accompanied by SWC variations, the question as to whether SWSIC and SWC share similar spatiotemporal features deserves further investigations. This is pertinent to the transferability of the knowledge gained from numerous SWC studies to understand the spatiotemporal variability in SWSIC. A number of statistical techniques have been developed to characterize spatiotemporal dynamics of SWC (Vereecken et al., 2014), among which two methods are most widely used. One is temporal stability analysis (TSA) (see the review by Vanderlinden et al. (2012)). As introduced by Vachaud et al. (1985), the TSA method is based on field observations that the SWC spatial structure tends to be temporally persistent, resulting in SWC at certain sites closer to and thus representative of the spatial mean (Hu et al., 2010; Dari et al., 2019). Another is to examine the relationship between the standard deviation (SD) and the spatial mean of SWC. Affected by a number of environmental factors (e.g., climate, vegetation, and soil), complex forms of this relationship were observed in the field (e.g., positive, negative, and upward convex relationships; Lawrence and Hornberger, 2007; Vereecken et al., 2007; Wang et al., 2017). The knowledge of these relationships can provide useful information for upscaling SWC and optimizing monitoring schemes (Famiglietti et al., 2008; Brocca et al., 2010). Therefore, we intended to examine SWSIC variations and analyze their environmental controls with the aid of classic statistical methods originally developed for analyzing SWC spatiotemporal patterns, which were expected to offer additional avenues for understanding SWSIC dynamics.

To this end, extensive field campaigns were conducted on a karst hillslope in Southwestern China, where the land surface is highly heterogeneous (Wang et al., 2019; Li et al., 2020), providing an ideal condition to study the spatiotemporal patterns of SWSIC. Owing to the complex ecohydrological processes in karst regions (Bakalowicz, 2005; Hartmann et al., 2014), SWSIC is an indispensable tool for revealing ecohydrological processes (Chen et al., 2017; Nie et al., 2019; Zhang et al., 2021). A comprehensive understanding of the spatiotemporal variability in SWSIC would be beneficial for improving the accuracy of SWSIC-based analyses in these regions (e.g., estimating the volume and ages of water stored in different compartments of the critical zone (Smith et al., 2020)). Meanwhile, although soil evaporation loss accounts for a relatively small proportion of precipitation in energy-limited regions, its impact on stable water isotopic compositions of stream water/groundwater cannot be ignored (Sprenger et al., 2017a) and significant fractionation signals in groundwater were observed in the study catchment (Zhao et al., 2018; Zhang et al., 2021). Given that the knowledge of variations in soil evaporation helps to calibrate rainfall-runoff models (see the review by Birkel and Soulsby (2015)), the spatiotemporal characteristics of kinetic fractionation signals of soil water were also investigated. In this study, 83 sampling points were set up on a karst hillslope, and seven sampling campaigns were conducted over a two-year period. Relevant environmental factors were also measured to evaluate their influences on the SWSIC spatiotemporal variations. The three aims of this study were: (1) to evaluate the overall spatiotemporal variations in SWSIC, (2) to investigate the controlling factors and processes of such variations, and (3) to examine whether the knowledge gained from SWC studies can be used to understand SWSIC spatiotemporal variations.

2. Methods and materials

2.1. Study area

The study area is located in Chenqi catchment with a drainage area of 1.25 km^2, which is part of the Puding Karst Ecosystem Research Station in Guizhou Province, Southwestern China (Fig. 1a). A wet subtropical monsoon climate is prevalent in this region with mean annual precipitation and temperature of 1341 mm and 15.2 ℃, respectively (Ni et al., 2017). Over 80% of annual precipitation occurs in wet season (from May to October). Hillslopes cover about 70% of the catchment area, and carbonate rock outcrops cover 10%–30% of the hillslope area (Zhang et al., 2019). Soils are thin and unevenly distributed with a mean soil depth of ~40 cm at our sampling site.

In this study, a southwest-facing hillslope with elevation from 1400 m to 1470 m and an average slope of ~20° was selected (Fig. 1a). The upper and middle sections of the hillslope (sampling points from *No*. 1 to *No*. 36 in Fig. 1b) are mainly covered by deciduous broadleaf trees (e.g., *Platycarya longipes*, *Kalopanax septemlobus*, and *Toona sinensis*) and understory shrubs and grasses, while the lower part (*No*. 37 to *No*. 83 in Fig. 1b) is primarily covered by sparse shrubs (e.g., *Pyracantha crenatoserrata* and *Coriaria nepalensis*) and grasses (e.g., *Heteropogon contortus* and *Pteridium revolutum*). Soils at the sampling points were found to be mainly composed of fine particles with respective average sand and clay content of 11.9% and 47.3%.

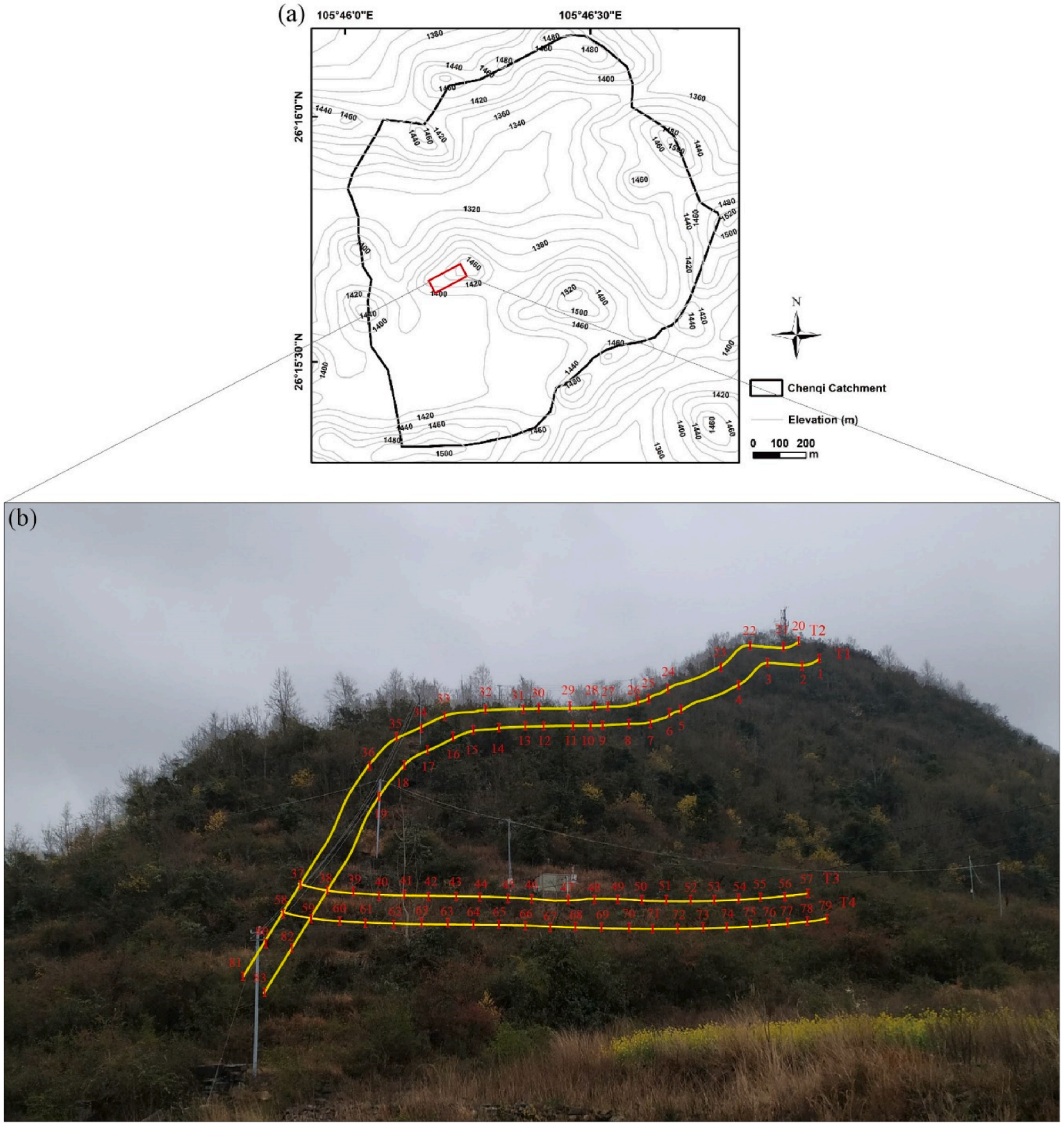

Fig. 1. Location map and sampling points distribution.

2.2. Field campaigns

As shown in Fig. 1b, two parallel transects along the hillslope (T1 and T2, ~6 m apart) and anther two transects perpendicular to the hillslope (T3 and T4, ~6 m apart) were established with a total of 83 sampling points. The length of T1 and T2 was ~190 m with an average spacing of ~9 m between neighboring points, while the length of T3 and T4 was ~64 m with ~3 m spacing between neighboring points. Seven sampling campaigns were conducted from March 2019 to December 2020 (Table 1). After removing surface litter from each sampling point, soil samples from shallow soil layers (0–10 cm) were collected using a 4-cm diameter hand auger. To reduce the impact of precipitation inputs on SWSIC, all soil samples were collected between 9:00 and 17:00 on non-rainy days within two days in each campaign. After excavations, soil samples were immediately placed in airtight bags and stored in a cooler box until lab analysis. During the study period, precipitation samples were collected by an automatic precipitation collector (5020, Qingdao Laoying Environmental Technology Co., Ltd, China) at the Puding Karst Ecosystem Research Station, which is about 5 km away from the study area. The collected rainfall samples were stored at 4 °C until lab analysis.

Table 1
Information of sampling campaigns.

No	Sampling date (mm/dd/yy)	Time since last large precipitation event (with P > 10 mm/d) (days)	Accumulative precipitation in two weeks before sampling (mm)
1	3/9/2019	37	9.7
2	6/4/2019	6	81.3
3	9/1/2019	18	15.0
4	12/8/2019	51	19.8
5	5/13/2020	2	69.1
6	8/19/2020	1	141.4
7	12/20/2020	66	12.0

To investigate the impacts of environmental factors on the spatio-temporal variability in SWSIC, relevant factors were also measured. Specifically, the slope at each point was estimated with the Level tool on smartphones. Soil depths were measured with a 2-cm diameter iron braze at five locations around each sampling point before the field campaigns began. The leaf area index (LAI) at each point was measured with LAI-2200C (Li-Cor, Lincoln NE, USA) during the peak growing season (e.g., August 2020).

2.3. Lab analysis

For stable water isotope analysis, soil water was extracted from the

collected soil samples by an automatic cryogenic vacuum extraction system (LI-2100, LICA United Technology Limited, China). After extraction, soil samples were oven-dried at 105 ℃ for 24 h and then weighed to calculate the extraction ratio (defined as the weight of extracted water divided by the total water loss after oven-drying). To minimize the impact of fractionation during soil water extraction, the extraction duration and temperature were experimentally predetermined using local soil samples with varying SWC. In this study, the average extraction ratio was over 98.3%, which was similar to previously reported values (Orlowski et al., 2018; Dai et al., 2020).

Both soil water and precipitation samples were filtered by 0.45 μm pore-size cellulose acetate membranes and then analyzed using a Picarro L2140-i wavelength-scanned cavity ring-down spectroscopy (WS-CRDS) instrument (Picarro Inc., Sunnyvale, CA, USA) at School of Earth System Science, Tianjin University. Each sample was measured three times and three refence standards (GBW04458, GBW04459, and GBW04460) were used for calibration (see details in Han et al. (2020)). The final water stable isotopic compositions were reported in per mil (‰) relative to Vienna Standard Mean Ocean Water (V-SMOW) as:

$$\delta^{18}\mathrm{O} \text{ or } \delta\mathrm{D} = \left(\frac{\mathrm{R_{sample}}}{\mathrm{R_{standard}}} - 1\right) \times 1000 \quad (1)$$

where $\mathrm{R_{sample}}$ and $\mathrm{R_{standard}}$ are the $^{18}O/^{16}O$ (or D/H) ratio for a measured sample and a standard sample, respectively. The precision of the measurements is ±0.05‰ for $\delta^{18}O$ and ±0.4‰ for δD.

Gravimetric SWC for each sample was determined in this study. Soil samples at each point collected during different field campaigns were well mixed and used for analyzing soil properties. A standard sieve-pipette method was used to determine soil particle size distributions by weight. Specifically, rock fragment content (RFC) and coarse sand content were measured by dry sieving. Medium and fine sand, silt, and clay contents were determined by a hydrometer method. Considering the possible impact of soil organic carbon (SOC) on δD of soil water during cryogenic vacuum extraction (Orlowski et al., 2016), as well as its influence on soil water storage capacity (Olness and Archer, 2005), SOC at each point was also measured with a potassium dichromate heating method (Zhang et al., 2012).

2.4. Data analysis

2.4.1. Line-conditioned excess

Compared with analysis of δD or $\delta^{18}O$ alone, a dual-isotope approach with line-conditioned excess (lc-excess) is able to correct for the effects of temporal variability in precipitation isotopic compositions on the variability in SWSIC and reveal the processes governing SWSIC spatiotemporal variations (Landwehr and Coplen, 2006). Given that spatial variations in precipitation isotopic compositions can be neglected at plot scales, lc-excess is particularly suitable for describing the kinetic fractionation caused by soil evaporation (Sprenger et al., 2017a; Hasselquist et al., 2018). Moreover, although we did not collect throughfall samples at each point in this study, Deng et al. (2017) showed that the isotopic differences between precipitation and throughfall samples under different canopies were very small (<0.33‰ for $\delta^{18}O$), where the study area was also located in a karst region in Southwestern China with similar vegetation coverage. Therefore, we assume that it is reasonable to use lc-excess at our study site. Besides, some recent studies showed that lc-excess worked well to track the temporal and spatial variations in kinetic fractionations caused by soil evaporation at relatively small spatial scales in energy-limited regions (Sprenger et al., 2017a; b). For example, with lc-excess, Sprenger et al. (2017a) found the spatial patterns of fractionation signals across a small peatland drainage network with an area of 0.77 km^2, and showed that the corresponding signal was imprinted on the stream water.

Specifically, lc-excess, which describes the deviation of δD values from local meteoric water lines (LMWL; Dansgaard, 1964), is defined as:

$$lc-excess = \delta\mathrm{D} - a \times \delta^{18}\mathrm{O} - b \quad (2)$$

where a and b represent the slope and intercept of the LMWL, respectively. Water undergoing kinetic fractionation caused by evaporation has a negative lc-excess value in a dual-isotope space (Landwehr et al., 2014). Following Sprenger et al. (2017a), lc-excess was used here as an indication of kinetic fractionation signals, with the LMWL ($\delta D = 8.08 \times \delta^{18}O + 11.17$; Fig. 3) derived from 68 rainfall events from April 2019 to October 2020. The weighted lc-excess value of precipitation during the study period was about 0.4‰ and the uncertainty of lc-excess was roughly ±0.8‰, based on the precision of isotope analysis and the slope of the LMWL. Given the high collinearity between $\delta^{18}O$ and δD values both for precipitation and soil water samples (Fig. 1S), only δD and lc-excess data were analyzed and both referred to SWSIC in the following analysis.

2.4.2. Statistical analysis

The TSA method has been widely employed to study SWC dynamics across different spatiotemporal scales (Vachaud et al., 1985; Vanderlinden et al., 2012), based on the metric of relative difference (*RD*) of SWC:

$$RD_{\mathrm{ij}} = \frac{\theta_{ij}}{\overline{\theta_j}} - 1 \quad (3)$$

$$\overline{\theta_j} = \frac{1}{N} \times \sum_{i=1}^{N} \theta_{ij} \quad (4)$$

where θ_{ij} is the SWC at location *i* and time *j*, and $\overline{\theta_j}$is the spatial mean SWC at time *j*, and *N* is the number of observational locations. With *m* measurements over the study period, the mean relative difference (*MRD*) of SWC (MRD_{SWC}) at location *i* can be written as:

$$MRD_{SWCi} = \frac{1}{m} \times \sum_{j=1}^{m} RD_{ij} \quad (5)$$

The term *MRD* is used to describe the wetness condition at a location relative to the spatial mean over the study period with positive MRD_{SWC} values indicating wetter conditions. The temporal stability of SWC is described by the SD of *RD* (*SDRD*):

$$SDRD_{SWCi} = \left(\frac{1}{m} \times \sum_{j=1}^{m} (RD_{ij} - MRD_i)^2\right)^{1/2} \quad (6)$$

Locations with high temporal stability are indicated by low *SDRD* values. Following Zhao et al. (2010), the index of time stability (*ITS*) was used to identify the representative locations:

$$ITS_{SWCi} = \left(MRD_{SWCi}^2 + SDRD_{SWCi}^2\right)^{1/2} \quad (7)$$

In this study, the TSA method was extended to investigate the spatiotemporal characteristics of SWSIC. Note that positive *MRD* values of δD ($MRD_{\delta D}$) and lc-excess (MRD_{lc}) indicate that the deuterium is more depleted in water samples and water samples experience higher degrees of kinetic fractionation than the spatial average, respectively. Finally, the metrics of *MRD* and *SDRD* were used to investigate the spatiotemporal characteristics of SWC and SWSIC, and evaluate their influencing factors (e.g., soil properties, microtopography, and vegetation).

The relationship between the spatial mean ($\overline{\theta_j}$) and standard deviation of SWC (SD_θ) is routinely used to understand SWC variability under different climatic and wetness conditions for upscaling purposes (Famiglietti et al., 2008; Wang et al., 2017). Based on *N* locations on day *j*, SD_θcan be calculated as:

$$SD_{\theta(j)} = \left[\frac{1}{N} \times \sum_{i=1}^{N} (\theta_{ij} - \overline{\theta_j})^2\right]^{1/2} \quad (8)$$

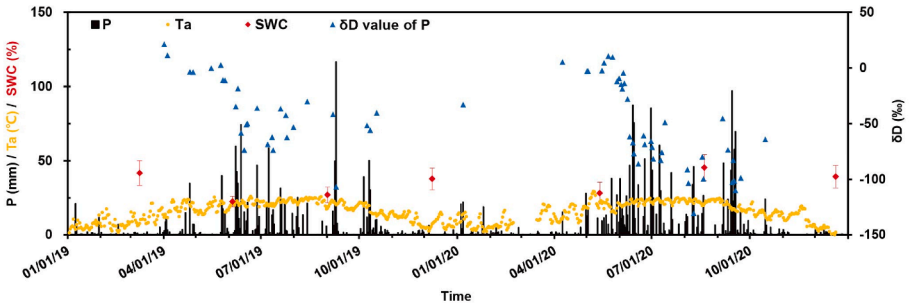

Fig. 2. Time series of precipitation (P), air temperature (Ta), δD value of P, and soil water content (SWC) during the study period. The error bar of SWC represents its standard deviation. The date is in mm/dd/yy in all figures.

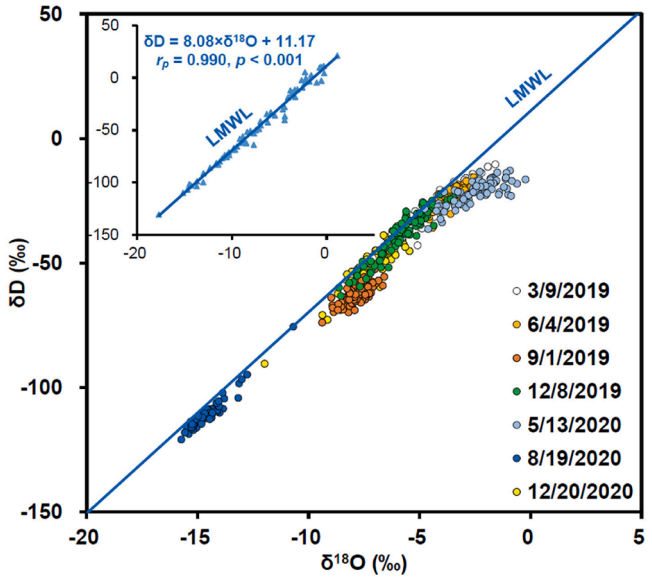

Fig. 3. Dual-isotope plot of precipitation and soil water samples. The inside smaller plot is for precipitation samples and the blue line is the fitted Local Mean Meteoric Line (LMWL). (For interpretation of the references to colour in this figure legend, the reader is referred to the web version of this article.)

By extending this relationship to estimate the spatial patterns of SWSIC, we intended to examine whether there would be similar scale effects for SWSIC variations.

3. Results and discussion

3.1. Overall spatiotemporal variations in SWSIC

Significant temporal variations in hydrometeorological conditions during the study period and spatial variations in point-specific properties were observed at the study site, providing an ideal opportunity to investigate spatiotemporal variations in SWSIC and associated influencing factors. Daily air temperature and precipitation along with corresponding δD values displayed clear seasonal variations (Fig. 2). Specifically, wet seasons from May to October were characterized by higher air temperature and precipitation (~81.4% of the total precipitation during the study period). In dry seasons and early wet seasons (e.g., May), deuterium was more enriched in precipitation, most likely due to different water vapor sources among different seasons (Liu et al., 2014). Environmental variables (e.g., microtopography, soil properties, and LAI) also showed significant spatial variations (Table 2). For example, the RFC varied between nil and 22.2%, while the clay content ranged from 10.6% to 70.2% at the study site, demonstrating the high heterogeneity of land surface conditions in karst regions (Wang et al., 2019).

The dual-isotope plot of precipitation and soil water samples is shown in Fig. 3. δD values in soil water (−121.0‰ ~ −10.5‰) exhibited a smaller range than those in precipitation (−130.7‰ ~ 21.3‰), suggesting that soil water was a mixture of different precipitation events (Penna et al., 2018; Dai et al., 2020). Most soil water data fell slightly below the LMWL, with the slope of the fitted soil evaporation line of about 7.73 (Fig. 1S), indicating relatively weaker soil evaporation in the study area as compared to that in midlatitudes and arid regions (Gibson et al., 2008). However, it does not mean that the effect of soil evaporation on SWSIC can be neglected in this study. For example, relatively strong soil evaporation was observed on May 13, 2020 with the spatial average lc-excess value of −12.8‰ (Table 3). More importantly, Fig. 3 provides strong field evidence of significant spatial variations in SWSIC at a field scale. As summarized in Table 3, the maximum and minimum ranges of δD values for soil water samples were 55.2‰ (December 20, 2020) and 20.3‰ (June 4, 2019), respectively, while the maximum and minimum ranges of lc-excess values were comparatively less with 26.2‰ (May 13, 2020) and 8.5‰ (August 19, 2020), respectively. Therefore, SWSIC data should be interpreted cautiously when their spatial variations are neglected (Goldsmith et al., 2018a; Penna et al., 2018; Beyer and Penna, 2021).

Fig. 3 and Table 3 show larger varying ranges of δD values of soil water in dry seasons (with the average range of 44.5‰; from November to April) than in wet seasons (with the average range of 27.6‰; from May to October), which could be primarily due to different degrees of soil water mixing (Pu et al., 2020). As displayed in Table 3, SWC also exhibited greater spatial variability in dry seasons than in wet seasons (except on August 19, 2020). In dry seasons, small rainfalls were not able to renew all stored water in soils and the large SWC spatial variations led to more uneven spatial distributions of δD values. Specifically, soils with

Table 2
Statistics of point-specific environmental variables.

	Soil depth (cm)	Slope (°)	RFC (%)	Sand (%)	Silt (%)	Clay (%)	SOC (%)	LAI
Max	80.0	47.0	22.2	35.8	55.7	70.2	4.5	4.2
Min	12.0	1.0	0.0	0.0	22.8	10.6	1.6	1.1
Average	38.3	11.1	6.9	11.9	40.8	47.3	2.4	2.4
SD	18.9	8.4	6.1	7.0	8.8	12.5	0.6	0.8

RFC-rock fragment content; SOC-soil organic carbon; LAI-leaf area index.

Table 3
Statistics of soil water content (SWC) and soil water stable isotopic compositions (δD and lc-excess).

mm/dd/yy	3/9/2019	6/4/2019	9/1/2019	12/8/2019	5/13/2020	8/19/2020	12/20/2020
	SWC (%)						
Max	64.1	30.8	40.0	61.2	53.8	74.5	56.9
Min	19.9	15.7	15.0	27.4	16.8	25.7	18.8
Average	41.6	22.4	27.0	37.8	28.2	45.3	39.2
SD	8.3	3.6	5.3	7.3	7.3	8.7	7.6
	δD (‰)						
Max	−10.5	−15.6	−52.6	−22.5	−12.9	−75.6	−35.3
Min	−48.1	−35.9	−73.9	−63.3	−36.4	−121.0	−90.5
Average	−29.6	−23.9	−63.1	−38.9	−21.8	−110.8	−51.1
SD	8.5	4.0	4.1	10.0	4.8	5.9	8.5
	lc-excess (‰)						
Max	2.7	0.0	−2.5	4.9	−0.9	−0.4	3.5
Min	−13.0	−12.4	−16.4	−11.3	−27.1	−8.9	−16.0
Average	−3.1	−4.8	−10.6	−3.0	−12.8	−4.1	−4.6
SD	3.3	2.8	3.0	3.0	5.4	1.7	3.7

higher water deficit would be more affected by newly input water, while those with lower water deficit would reflect more of the antecedent isotopic composition. By comparison, in wet seasons, with sufficient precipitation, soil water could be mostly replaced by recent rainfalls regardless of the storage capacity at each point (Zhang et al., 2021), leaving a relatively uniform δD distribution. Moreover, soil water in wet seasons was mostly consumed by root water uptake, which will usually not change the isotopic compositions of soil water (Nie et al., 2010; Zhao et al., 2018). Thus, the relatively uniform distribution of δD could be retained. However, there could also be some exceptions in wet seasons when there were extra water sources other than recent precipitation. For example, after a total of 141.4 mm precipitation in two weeks before the field campaign, a large variation (−121.0‰ ~ −75.6‰) in δD of soil water was observed on August 19, 2020. This could be attributed to the recharge from epikarst (Williams, 2008) for some points with coarser soil texture and close to a temporary spring outlet (e.g., point *No*.67 in Fig. 1b). Epikarst water in wet seasons is typically more enriched in heavy isotopes than recent precipitation (Perrin et al., 2003; Nie et al., 2010) and could thus increase the spatial variations in δD value of soil water. Overall, our results showed significant spatial variability in SWSIC even at field scales, which was temporally dynamic.

3.2. Temporal stability analysis of SWC and SWSIC

3.2.1. Characteristics of MRD and SDRD for SWC and SWSIC

To compare the temporal persistence of SWC and SWSIC spatial structures, the Spearman nonparametric test was employed and the correlation coefficients (r_s) between each pair of sampling campaigns are summarized in Table 4. Similar to previous findings in non-karst regions (e.g., Wang et al., 2015; Wu et al., 2020), the SWC spatial structures at our karst site also exhibited strong temporal persistence, with all $r_s \geq 0.371$ ($p < 0.001$), while the spatial structures of δD and lc-excess were less temporally stable with less than half of r_s values at $p < 0.05$.

The ranked MRD_{SWC}, $MRD_{\delta D}$, and MRD_{lc} with associated *SDRD* are plotted in Fig. 4, revealing differences in those *MRD* ranges. For instance, MRD_{SWC} from −25.0% to 45.1% was in line with previously reported ranges (Vanderlinden et al., 2012), while $MRD_{\delta D}$ showed a smaller range from −21.4% to 28.8%. By comparison, MRD_{lc} varied from −79.2% to 93.2%, indicating high spatial variability in kinetic fractionation signals and underscoring the necessity to examine the spatial variability in soil evaporation even at field scales in humid regions (Sprenger et al., 2017a). Meanwhile, it should be noted that here the variation is a relative value to the spatial average condition and large spatial variations in lc-excess does not mean that the overall soil evaporation is strong. The much smaller varying ranges of $MRD_{\delta D}$ than MRD_{lc} implied that soil evaporation heterogeneity might not be the primary reason for spatial variations in δD value of soil water in this study. Additionally, combining with the relative smaller isotopic differences between throughfall samples under contrasting canopies in a similar region (Deng et al., 2017), we supposed that differences in mixing degrees of water source in soil might be responsible for such variations in soil water δD values (Goldsmith et al., 2018a). Besides, compared with points with shrubs and grass, points with deciduous trees exhibited higher rankings of MRD_{SWC} (wetter conditions) and $MRD_{\delta D}$ (more negative δD values). With sufficient precipitation input, SWC at our study site was mainly controlled by soil storage capacities (Lawrence

Table 4
Spearman's rank correlation coefficient (r_s) between sampling campaigns.

	mm/dd/yy	3/9/2019	6/4/2019	9/1/2019	12/8/2019	5/13/2020	8/19/2020	12/20/2020
SWC	3/9/2019	1.000	0.583***	0.550***	0.560***	0.672***	0.371***	0.486***
	6/4/2019		1.000	0.574***	0.739***	0.642***	0.465***	0.535***
	9/1/2019			1.000	0.610***	0.557***	0.439***	0.495***
	12/8/2019				1.000	0.704***	0.469***	0.537***
	5/13/2020					1.000	0.472***	0.552***
	8/19/2020						1.000	0.449***
	12/20/2020							1.000
δD	3/9/2019	1.000	0.372***	0.077	0.371***	−0.122	−0.054	0.169
	6/4/2019		1.000	0.254*	0.292**	0.007	0.051	0.294**
	9/1/2019			1.000	0.254*	0.179	0.208	0.362***
	12/8/2019				1.000	0.030	0.128	0.404***
	5/13/2020					1.000	0.335**	−0.151
	8/19/2020						1.000	0.294**
	12/20/2020							1.000
lc-excess	3/9/2019	1.000	0.434***	0.222*	0.261*	−0.023	−0.055	0.155
	6/4/2019		1.000	0.332**	0.224*	0.198	0.148	0.075
	9/1/2019			1.000	0.445***	0.287**	0.385***	0.055
	12/8/2019				1.000	0.135	0.184	0.375***
	5/13/2020					1.000	0.188	−0.125
	8/19/2020						1.000	−0.090
	12/20/2020							1.000

* $p < 0.05$; ** $p < 0.01$; *** $p < 0.001$.

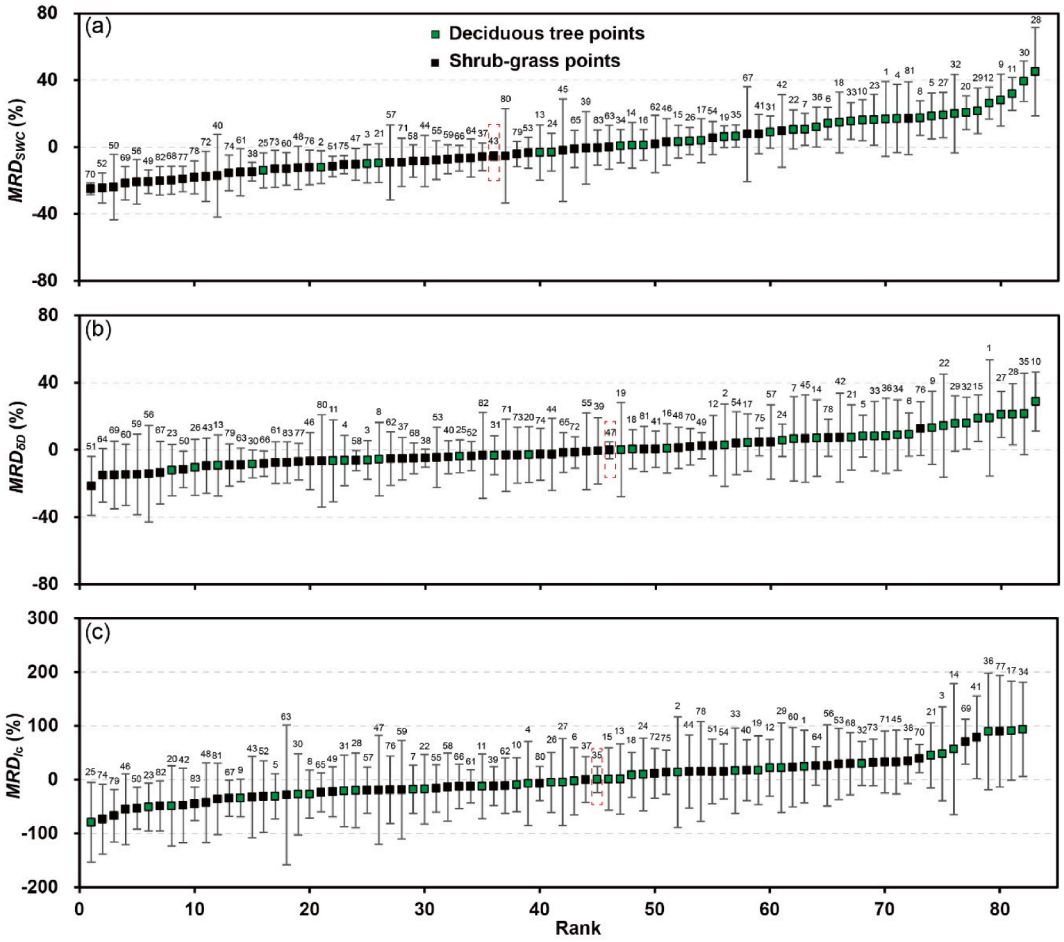

Fig. 4. Ranked *MRD* with associated *SDRD* (vertical bars) of (a) soil water content (SWC), (b) δD, and (c) lc-excess. The dotted frames indicate the identified representative points based on corresponding minimal *ITS* (the index of temporal stability) values.

and Hornberger, 2007). Therefore, wetter conditions at deciduous-tree points could be attributed to higher SOC and clay content (Table 1S; Olness and Archer, 2005). The more negative δD values at deciduous-tree points might be related to (1) the tree shading effect, which could lower soil evaporation intensity and leave less enriched δD values in residual soil water (Raz-Yaseef et al., 2010) and/or (2) canopy interceptions of small rainfalls with enriched isotopic compositions (Fig. 2S; Kato et al., 2013). Moreover, compared to $SDRD_{SWC}$ (averaged at 12.8%), $SDRD_{\delta D}$ (16.6%) and $SDRD_{lc}$ (61.4%) showed less temporal stability. Overall, the results revealed the contrasts in the spatiotemporal patterns of SWC and SWSIC, the latter of which was temporally more dynamic.

3.2.2. Controls on the spatial variations in SWC and SWSIC

Given the high correlations between environmental variables (Table 2S), partial rank correlation analysis (r_{pr}) was used to evaluate their impacts on the spatial variations in SWC, δD, and lc-excess values (Table 5). Similar to previous studies (Vereecken et al., 2014), MRD_{SWC} at the study points was predominantly influenced by soil properties, e.g., positive correlations of MRD_{SWC} with SOC ($r_{pr} = 0.663$ and $p < 0.001$) and clay content ($r_{pr} = 0.287$ and $p = 0.012$).

As shown in Table 5, $MRD_{\delta D}$ and MRD_{lc} significantly correlated only with RFC, whereas MRD_{SWC} was correlated instead with SOC and clay content. The negative correlation between MRD_{lc} and RFC (r_{pr} = -0.226 and $p = 0.050$) implied that points with higher RFC experienced less degrees of kinetic fractionation. There might be two opposite impacts of RFC on soil evaporation: (1) the low specific heat storage capacity of rock fragments might lead to the heating of soils and therefore increase soil evaporation (Cousin et al., 2003), and (2) the high RFC may increase soil hydraulic conductivity and thus reduce the mean residence time of soil water and lower its possibility to be evaporated (Wang et al., 2009). The negative MRD_{lc} - RFC correlation suggests that the latter effect was predominant in this study. Meanwhile, the correlation between $MRD_{\delta D}$ and RFC was also negative ($r_{pr} = -0.257$ and $p = 0.025$), indicating that the deuterium of soil water was more enriched at points with higher RFC. Since the points with higher RFC were associated with lower LAI (Table 2S) and δD values of precipitation were negatively correlated with its amount (Fig. 2S), it was speculated that the more enriched

Table 5
Partial rank correlation coefficient (r_{pr}) between environmental variables and the *MRD* of SWC, δD, and lc-excess.

		Soil depth (cm)	Slope (°)	RFC (%)	Sand (%)	Silt (%)	Clay (%)	SOC (%)	LAI
r_{pr}	MRD_{SWC}	−0.167	−0.142	−0.087	−0.219	−0.165	**0.287***	**0.663*****	0.018
	$MRD_{\delta D}$	0.083	0.143	**−0.257***	0.209	0.106	0.177	0.138	−0.078
	MRD_{lc}	−0.083	0.13	**−0.226***	−0.05	−0.083	−0.038	−0.199	−0.081

* $p < 0.05$; $^{**}p < 0.01$; $^{***}p < 0.001$.

deuterium of soil water at the points with high RFC was likely owing to the higher throughfall of small precipitation events with enriched deuterium (Kato et al., 2013). Monitoring of isotopic compositions of input water at finer spatial scales may shed light on a better understanding of SWSIC spatial patterns in future studies (Goldsmith et al., 2018a). Some previous studies showed that δD values of soil water could be influenced by SOC owing to the dynamic exchange of deuterium between organic matter and liquid water during cryogenic extractions (Orlowski et al., 2016; Chen et al., 2020); however, no evidence of such effect was found in our study with $r_{pr} = 0.138$ and $p = 0.233$ for $MRD_{\delta D}$ -SOC relationship. A similar phenomenon was also observed in natural field soils (Goldsmith et al., 2018b), showing that the effect of soil physiochemical compositions on water isotopic fractionation in complex natural soils needs further investigations.

Although δD and lc-excess exhibited different spatiotemporal characteristics from those of SWC as shown above, their most representative monitoring point can still be identified based on *ITS* metrics. Relationships between the spatial mean and measured values from each representative point are displayed in Fig. 5. Generally, good linear correlations were found for these three variables with $r_p \geq 0.968$ ($p < 0.001$), demonstrating that TSA method could be used to select representative monitoring points for both SWC and SWSIC. To further demonstrate the features of representative points for SWC and SWSIC, eight points (~10% of the total 83 points) with lowest *ITS* values were picked for SWC, δD, and lc-excess. It was found that those points for SWC (e.g., *No*. 43, 79, 26, 19, 35, 16, 53, and 34 in Fig. 1b) were located at flatter slopes with soil textures close to the spatial mean, which was consistent with previous results (e.g., Zhang and Shao, 2013; Dari et al., 2019). By contrast, the points for δD (*No*. 47, 38, 49, 58, 52, 57, 75, and 68 in Fig. 1b) had coarser soil textures. Note that no general characteristics could be inferred from the points for lc-excess (e.g., *No*. 35, 80, 61, 39, 18, 37, 66, and 75). Clearly, in spite of previous (e.g., Goldsmith et al. (2018a)) and our efforts, future investigation is still needed to fully understand how environmental controls drive the temporal evolution of SWSIC spatial structures.

3.3. Relationships between the spatial mean and variability in SWC and SWSIC

Relationships between the spatial mean and SD of SWC, δD, and lc-excess are compared in Fig. 6. A positive relationship was observed for SWC (Fig. 6a), indicating that the spatial variability in SWC increased with soil wetness conditions in the study area. This was different from the common notion that SWC variability decreases with increasing wetness conditions in humid regions (Lawrence and Hornberger, 2007), which could be due to the large heterogeneity in soil properties among the sampling points (Table 2). By comparison, probably owing to the contrasting isotopic compositions of input water in different seasons, no clear relationship was found between the spatial mean and SD of δD in this study (Fig. 6b). The negative correlation between the spatial mean and SD of lc-excess in Fig. 6c demonstrated that the corresponding spatial variations increased with mean kinetic fractionation signals, which was similar to the result of soil evaporation spatial analysis at an energy-limited peatland drainage network (Sprenger et al., 2017a). Although this negative correlation was not statistically significant ($r_p = -0.634$ and $p = 0.127$), it could have important implications for understanding the scale effect of soil evaporation variations and could be helpful in monitoring network design. In future studies, more temporally intensive samplings are needed to fully capture its spatial patterns.

Considering that actual evapotranspiration was mainly limited by evaporative demands in humid subtropical climate regions (Zhang et al., 2018), the impact of mean potential evapotranspiration of 14 days (PET_{14}) prior to each sampling campaign on the spatial mean and SD of lc-excess was analyzed (Fig. 7). Daily potential evapotranspiration was calculated by the Penman-Monteith equation (Allen et al., 1998) and PET_{14} was taken as a measure of antecedent potential evaporation, which was not partitioned into potential evaporation and transpiration, since previous studies showed a linear correlation between evaporation and transpiration in subtropical climates (Zhang et al., 2018). Note that the impacts of PET_7 and PET_{30} were similar (Fig. 3S) and thus are not reported here. Fig. 7 shows that when PET_{14} was high (e.g., >2 mm/d), mean lc-excess decreased with PET_{14} while its SD increased with PET_{14}, suggesting that the variability increased with mean kinetic fractionation under relatively higher evaporative demand conditions. The higher spatial variability in kinetic fractionation under high evaporative demand conditions might be linked to the greater energy availability differences caused by shading effects of vegetation and exposed bare rocks (Raz-Yaseef et al., 2010; Li et al., 2014; Zhao et al., 2015). Interestingly, when PET_{14} was low (e.g., <2 mm/d), there was also a slight decrease of mean lc-excess as PET_{14} decreased, accompanied by increasing spatial variations. According to Sprenger et al. (2017b), this could be related to the delayed response of lc-excess to the onset of soil evaporation in lower evaporative demand conditions. Overall, these results provided valuable information for soil evaporation monitoring network design.

4. Conclusions

In this study, based on data from extensive field campaigns on a karst hillslope, the spatiotemporal characteristics of soil water stable isotopic composition (SWSIC) and corresponding controlling factors were compared to those of soil water content (SWC). Generally, SWSIC showed considerable spatiotemporal variations with more complex patterns than SWC. The results of the temporal stability analysis (TSA) showed that compared with SWC: (1) δD values exhibited smaller spatial variations, while lc-excess values displayed considerably larger ones, suggesting that processes other than soil evaporation heterogeneity, such as differences in mixing degrees of water source in soil, might be

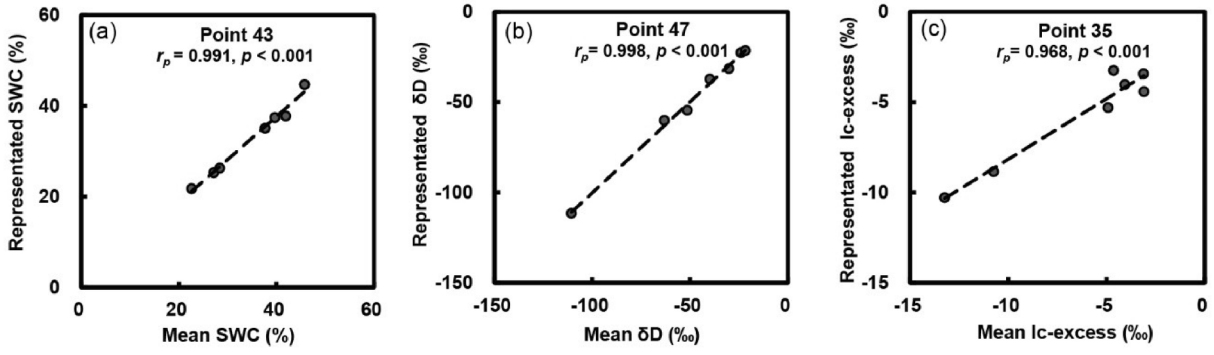

Fig. 5. Comparisons between the spatial mean of (a) soil water content (SWC), (b) δD, and (c) lc-excess with corresponding values from the most representative point. r_p is Pearson's correlation coefficient.

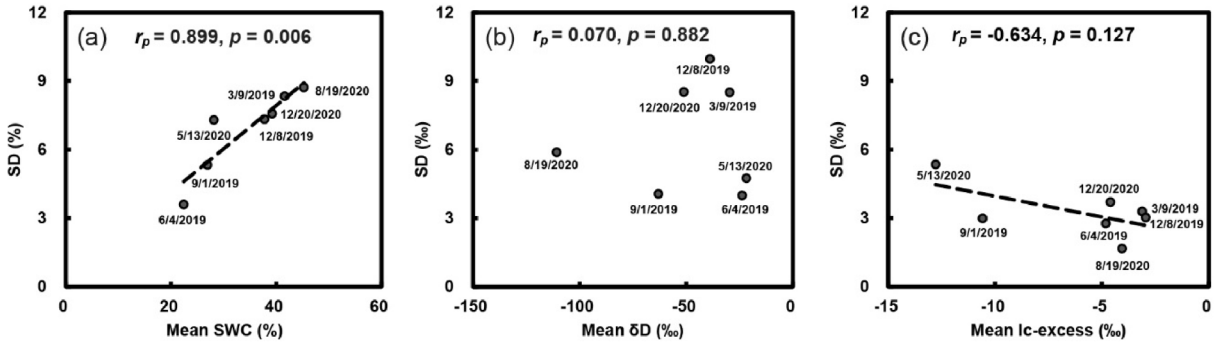

Fig. 6. Correlations between the spatial mean and associated standard deviation (SD) of (a) soil water content (SWC), (b) δD, and (c) lc-excess.

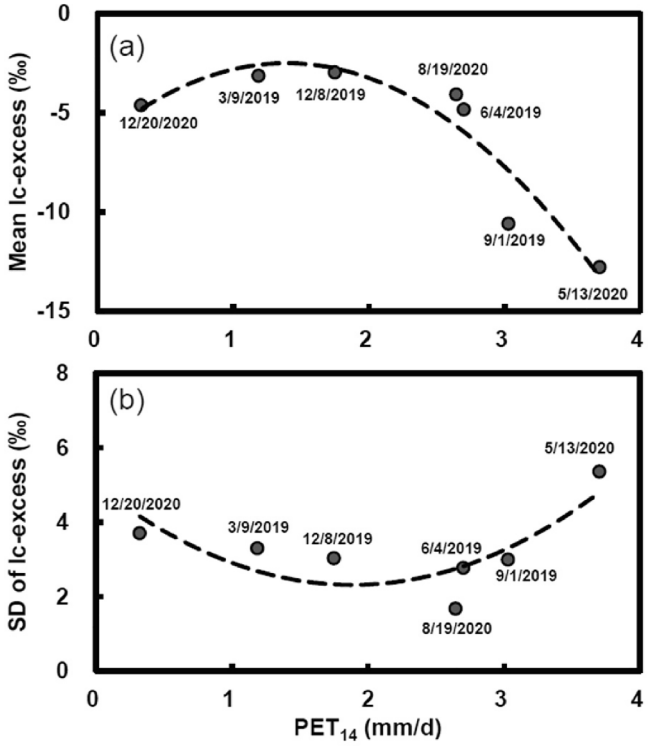

Fig. 7. Correlations between the mean potential evapotranspiration of 14 days prior to each sampling campaign (PET_{14}) with (a) mean lc-excess, (b) SD of lc-excess. The dashed lines are the fitted polynomial curves.

primarily responsible for the spatial variations in δD value of soil water; (2) the spatial structures of SWSIC were temporally less stable, reflecting the joint effects of complex land surface processes and isotopic compositions of input water on SWSIC dynamics; (3) the spatiotemporal variations in SWSIC were less explained by environmental variables that were also contrasted to those of SWC, suggesting that the knowledge obtained from SWC spatiotemporal studies might not be directly transferable to understand SWSIC variations; and (4) the TSA method could be used to select representative monitoring points for SWSIC. The results of this study provided additional insights into understanding the spatiotemporal characteristics of SWSIC, which in turn is critical for more accurately deciphering relevant ecohydrological processes.

CRediT authorship contribution statement

Qin Liu: Conceptualization, Methodology, Writing – original draft, Writing – review & editing. **Tiejun Wang:** Conceptualization, Funding acquisition, Supervision, Writing – original draft, Writing – review & editing. **Cong-qiang Liu:** Conceptualization, Project administration, Writing – original draft, Writing – review & editing. **Espoire M.R.B. Mikouendanandi:** Writing – original draft, Writing – review & editing. **Xi Chen:** Funding acquisition, Writing – review & editing. **Tao Peng:** Investigation, Writing – original draft. **Lin Zhang:** Investigation, Writing – original draft.

Declaration of Competing Interest

The authors declare that they have no known competing financial interests or personal relationships that could have appeared to influence the work reported in this paper.

Acknowledgement

This work was supported by the National Natural Scientific Foundation of China (42171036, U1612441). The authors would like to acknowledge the financial support from Tianjin University for this study, and T. Wang also acknowledges the financial support from the Thousand Talent Program for Young Outstanding Scientists for this study. The authors also thank Prof. James Kirchner from ETH for his constructive comments and English editing during revision process.

Appendix A. Supplementary data

Supplementary data to this article can be found online at https://doi.org/10.1016/j.jhydrol.2022.127964.

References

Allen, R.G., Pereira, L.S., Raes, D., Smith, M., 1998. Crop evapotranspiration - Guidelines for computing crop water requirements - FAO Irrigation and drainage paper 56.
Bakalowicz, M., 2005. Karst groundwater: a challenge for new resources. Hydrogeol. J. 13 (1), 148–160.
Barbeta, A., Gimeno, T.E., Clave, L., Frejaville, B., Jones, S.P., Delvigne, C., et al., 2020. An explanation for the isotopic offset between soil and stem water in a temperate tree species. New Phytologist 227 (3), 766–779.
Beyer, M., Penna, D., 2021. On the spatio-temporal under-representation of isotopic data in ecohydrological studies. Front. Water 3, 643013.
Birkel, C., Soulsby, C., 2015. Advancing tracer-aided rainfall-runoff modelling: a review of progress, problems and unrealised potential. Hydrol. Process. 29 (25), 5227–5240.
Brocca, L., Melone, F., Moramarco, T., Morbidelli, R., 2010. Spatial-temporal variability of soil moisture and its estimation across scales. Water Resour. Res. 46 (2).
Chen, H., Hu, K., Nie, Y., Wang, K., 2017. Analysis of soil water movement inside a foot slope and a depression in a karst catchment, Southwest China. Sci. Rep. 7 (1), 2544.
Chen, Y., Helliker, B., Tang, X., Li, F., Zhou, Y., Song, X., 2020. Stem water cryogenic extraction biases estimation in deuterium isotope composition of plant source water. In: Proceedings of the National Academy of Sciences, p. 202014422.
Cousin, I., Nicoullaud, B., Coutadeur, C., 2003. Influence of rock fragments on the water retention and water percolation in a calcareous soil. Catena 53 (2), 97–114.
Dai, J., Zhang, X., Luo, Z., Wang, R., Liu, Z., He, X., et al., 2020. Variation of the stable isotopes of water in the soil-plant-atmosphere continuum of a Cinnamomum camphora woodland in the East Asian monsoon region. J. Hydrol. 589, 125199.
Dansgaard, W., 1964. Stable isotopes in precipitation. Tellus 16 (4), 436–468.
Dari, J., Morbidelli, R., Saltalippi, C., Massari, C., Brocca, L., 2019. Spatial-temporal variability of soil moisture: addressing the monitoring at the catchment scale. J. Hydrol. 570, 436–444.

Demand, D., Blume, T., Weiler, M., 2019. Spatio-temporal relevance and controls of preferential flow at the landscape scale. Hydrol. Earth Syst. Sci. 23 (11), 4869–4889.
Deng, Y., Jiang, Z., Kuo, Y.-M., Zhou, X., 2017. Effects of canopy interception on epikarst water chemistry and its response to precipitation in Southwest China. Carbonates Evaporites 34 (2), 273–282.
Evaristo, J., Jasechko, S., Mcdonnell, J.J., 2015. Global separation of plant transpiration from groundwater and streamflow. Nature 525 (7567), 91–94.
Famiglietti, J.S., Ryu, D., Berg, A.A., Rodell, M., Jackson, T.J., 2008. Field observations of soil moisture variability across scales. Water Resour. Res. 44, W01423.
Gazis, C., Feng, X., 2004. A stable isotope study of soil water: evidence for mixing and preferential flow paths. Geoderma 119 (1–2), 97–111.
Gibson, J.J., Birks, S.J., Edwards, T.W.D., 2008. Global prediction of δ_A and δ^2H-$\delta^{18}O$ evaporation slopes for lakes and soil water accounting for seasonality. Global Biogeochem. Cycles 22, GB2031.
Goldsmith, G.R., Allen, S.T., Braun, S., Engbersen, N., Romero González-Quijano, C., Kirchner, J.W., et al., 2018a. Spatial variation in throughfall, soil, and plant water isotopes in a temperate forest. Ecohydrology 12, e2059.
Goldsmith, G.R., Allen, S.T., Braun, S., Engbersen, N., Gonzalez-Quijano, C.R., Kirchner, J.W., et al., 2018b. Data from: Spatial variation in throughfall, soil, and plant water isotopes in a temperate forest. Dryad Digital Repository.
Han, X., Lang, Y., Wang, T., Liu, C.Q., Li, F., Wang, F., et al., 2020. Temporal and spatial variations in stable isotopic compositions of precipitation during the typhoon Lekima (2019), China. Sci. Total Environ. 762, 143143.
Hartmann, A., Goldscheider, N., Wagener, T., Lange, J., Weiler, M., 2014. Karst water resources in a changing world: review of hydrological modeling approaches. Rev. Geophys. 52 (3), 218–242.
Hasselquist, N.J., Benegas, L., Roupsard, O., Malmer, A., Ilstedt, U., 2018. Canopy cover effects on local soil water dynamics in a tropical agroforestry system: evaporation drives soil water isotopic enrichment. Hydrol. Process. 32 (8), 994–1004.
Hu, W., Shao, M., Han, F., Reichardt, K., Tan, J., 2010. Watershed scale temporal stability of soil water content. Geoderma 158 (3–4), 181–198.
Kato, H., Onda, Y., Nanko, K., Gomi, T., Yamanaka, T., Kawaguchi, S., 2013. Effect of canopy interception on spatial variability and isotopic composition of throughfall in Japanese cypress plantations. J. Hydrol. 504, 1–11.
Kleine, L., Tetzlaff, D., Smith, A., Wang, H., Soulsby, C., 2020. Using water stable isotopes to understand evaporation, moisture stress, and re-wetting in catchment forest and grassland soils of the summer drought of 2018. Hydrol. Earth Syst. Sci. 24 (7), 3737–3752.
Landwehr, J.M., Coplen, T.B., 2006. Line-conditioned excess: a new method for characterizing stable hydrogen and oxygen isotope ratios in hydrologic systems. Int. Conf. Isotopes Environ. Stud. 132–135.
Landwehr, J.M., Coplen, T.B., Stewart, D.W., 2014. Spatial, seasonal, and source variability in the stable oxygen and hydrogen isotopic composition of tap waters throughout the USA. Hydrol. Process. 28 (21), 5382–5422.
Lawrence, J.E., Hornberger, G.M., 2007. Soil moisture variability across climate zones. Geophys. Res. Lett. 34, L20402.
Li, S., Ren, H.D., Xue, L., Chang, J., Yao, X.H., 2014. Influence of bare rocks on surrounding soil moisture in the karst rocky desertification regions under drought conditions. Catena 116, 157–162.
Li, S.-L., Xu, S., Wang, T.-J., Yue, F.-J., Peng, T., Zhong, J., et al., 2020. Effects of agricultural activities coupled with karst structures on riverine biogeochemical cycles and environmental quality in the karst region. Agric. Ecosyst. Environ. 303, 107120.
Liu, J., Song, X., Yuan, G., Sun, X., Yang, L., 2014. Stable isotopic compositions of precipitation in China. Tellus B: Chem. Phys. Meteorol. 66 (1), 22567.
Liu, Q., Wang, T.-J., Han, Q., Sun, S.-B., Liu, C.-Q., Chen, X., 2019. Diagnosing environmental controls on actual evapotranspiration and evaporative fraction in a water-limited region from northwest China. J. Hydrol. 578, 124045.
Ni, J., Wang, S.J., Liu, Y.B., Cai, X.L., Cheng, A.Y., Peng, T., et al., 2017. Establishment and monitoring of biological plots at Puding Karst ecosystem research station. Earth Environ. 45 (1), 10–113. In Chinese.
Nie, Y.-P., Chen, H.-S., Wang, K.-L., Tan, W., Deng, P.-Y., Yang, J., 2010. Seasonal water use patterns of woody species growing on the continuous dolostone outcrops and nearby thin soils in subtropical China. Plant Soil 341 (1–2), 399–412.
Nie, Y.-P., Chen, H.-S., Ding, Y.-L., Zou, Q.-Y., Wang, K.-L., 2019. Qualitative identification of hydrologically different water sources used by plants in rock-dominated environments. J. Hydrol. 573, 386–394.
Oerter, E.J., Bowen, G.J., 2019. Spatiotemporal heterogeneity in soil water stable isotopic composition and its ecohydrologic implications in semi-arid ecosystems. Hydrol. Process. 33, 1724–1738.
Olness, A., Archer, D., 2005. Effect of organic carbon on available water in soil. Soil Sci. 170 (2), 90–101.
Orlowski, N., Breuer, L., Angeli, N., Boeckx, P., Brumbt, C., Cook, C.S., et al., 2018. Inter-laboratory comparison of cryogenic water extraction systems for stable isotope analysis of soil water. Hydrol. Earth Syst. Sci. 22 (7), 3619–3637.
Orlowski, N., Breuer, L., McDonnell, J.J., 2016. Critical issues with cryogenic extraction of soil water for stable isotope analysis. Ecohydrology 9 (1), 3–10.
Oshun, J., Dietrich, W.E., Dawson, T.E., Fung, I., 2016. Dynamic, structured heterogeneity of water isotopes inside hillslopes. Water Resour. Res. 52, 164–189.
Penna, D., Hopp, L., Scandellari, F., Allen, S.T., Benettin, P., Beyer, M., et al., 2018. Ideas and perspectives: tracing terrestrial ecosystem water fluxes using hydrogen and oxygen stable isotopes – challenges and opportunities from an interdisciplinary perspective. Biogeosciences 15 (21), 6399–6415.
Penna, D., van Meerveld, H.J., 2019. Spatial variability in the isotopic composition of water in small catchments and its effect on hydrograph separation. WIREs Water 6 (5), e1367.
Perrin, J., Jeannin, P.-Y., Zwahlen, F., 2003. Epikarst storage in a karst aquifer: a conceptual model based on isotopic data, Milandre test site, Switzerland. J. Hydrol. 279 (1–4), 106–124.
Pu, H., Song, W., Wu, J., 2020. Using soil water stable isotopes to investigate soil water movement in a water conservation forest in Hani Terrace. Water 12 (12), 3520.
Quade, M., Brüggemann, N., Graf, A., Vanderborght, J., Vereecken, H., Rothfuss, Y., 2018. Investigation of kinetic isotopic fractionation of water during bare soil evaporation. Water Resour. Res. 54 (9), 6909–6928.
Raz-Yaseef, N., Rotenberg, E., Yakir, D., 2010. Effects of spatial variations in soil evaporation caused by tree shading on water flux partitioning in a semi-arid pine forest. Agric. For. Meteorol. 150 (3), 454–462.
Rothfuss, Y., Javaux, M., 2017. Reviews and syntheses: Isotopic approaches to quantify root water uptake: a review and comparison of methods. Biogeosciences 14 (8), 2199–2224.
Seneviratne, S.I., Corti, T., Davin, E.L., Hirschi, M., Jaeger, E.B., Lehner, I., et al., 2010. Investigating soil moisture–climate interactions in a changing climate: a review. Earth Sci. Rev. 99 (3–4), 125–161.
Smith, A., Tetzlaff, D., Kleine, L., Maneta, M.P., Soulsby, C., 2020. Isotope-aided modelling of ecohydrologic fluxes and water ages under mixed land use in Central Europe: the 2018 drought and its recovery. Hydrol. Process. 34 (16), 3406–3425.
Sprenger, M., Leistert, H., Gimbel, K., Weiler, M., 2016. Illuminating hydrological processes at the soil-vegetation-atmosphere interface with water stable isotopes. Rev. Geophys. 54 (3), 674–704.
Sprenger, M., Tetzlaff, D., Tunaley, C., Dick, J., Soulsby, C., 2017a. Evaporation fractionation in a peatland drainage network affects stream water isotope composition. Water Resour. Res. 53 (1), 851–866.
Sprenger, M., Tetzlaff, D., Soulsby, C., 2017b. Soil water stable isotopes reveal evaporation dynamics at the soil–plant–atmosphere interface of the critical zone. Hydrol. Earth Syst. Sci. 21 (7), 3839–3858.
Sprenger, M., Stumpp, C., Weiler, M., Aeschbach, W., Allen, S.T., Benettin, P., et al., 2019. The demographics of water: a review of water ages in the critical zone. Rev. Geophys. 57, 800–834.
Thomas, E.M., Lin, H., Duffy, C.J., Sullivan, P.L., Holmes, G.H., Brantley, S.L., et al., 2013. Spatiotemporal patterns of water stable isotope compositions at the shale hills critical zone observatory: linkages to subsurface hydrologic processes. Vadose Zone J. 12 (4), 1–6.
Troch, P.A., Carrillo, G.A., Heidbüchel, I., Rajagopal, S., Switanek, M., Volkmann, T.H. M., et al., 2009. Dealing with landscape heterogeneity in watershed hydrology: a review of recent progress toward new hydrological theory. Geogr. Compass 3 (1), 375–392.
Vachaud, G., Silans, A.P.D., Balabanis, P., Vauclin, M., 1985. Temporal stability of spatially measured soil water probability density function. Soil Sci. Soc. Am. J. 49 (4), 822–828.
Vanderlinden, K., Vereecken, H., Hardelauf, H., Herbst, M., Martínez, G., Cosh, M.H., et al., 2012. Temporal stability of soil water contents: a review of data and analyses. Vadose Zone Journal, 11(4): vzj2011.0178.
Vereecken, H., Kamai, T., Harter, T., Kasteel, R., Hopmans, J., Vanderborght, J., 2007. Explaining soil moisture variability as a function of mean soil moisture: a stochastic unsaturated flow perspective. Geophys. Res. Lett. 34, L22402.
Vereecken, H., Huisman, J.A., Bogena, H., Vanderborght, J., Vrugt, J.A., Hopmans, J.W., 2008. On the value of soil moisture measurements in vadose zone hydrology: a review. Water Resour. Res. 44, W00D06.
Vereecken, H., Huisman, J.A., Pachepsky, Y., Montzka, C., van der Kruk, J., Bogena, H., et al., 2014. On the spatio-temporal dynamics of soil moisture at the field scale. J. Hydrol. 516, 76–96.
Wang, K., Zhang, C., Chen, H., Yue, Y., Zhang, W., Zhang, M., et al., 2019. Karst landscapes of China: patterns, ecosystem processes and services. Landscape Ecol. 34 (12), 2743–2763.
Wang, T., Istanbulluoglu, E., Lenters, J., Scott, D., 2009. On the role of groundwater and soil texture in the regional water balance: an investigation of the Nebraska Sand Hills, USA. Water Resour. Res. 45, W04412.
Wang, T., Liu, Q., Franze, T.E., Li., R., Lang, Y., Fiebrich, C., 2017. Spatial patterns of soil moisture from two regional monitoring networks in the United States. J. Hydrol. 552, 578–585.
Wang, T., Wedin, D.A., Franz, T.E., Hiller, J., 2015. Effect of vegetation on the temporal stability of soil moisture in grass-stabilized semi-arid sand dunes. J. Hydrol. 521, 447–459.
Williams, P.W., 2008. The role of the epikarst in karst and cave hydrogeology_ a review. Int. J. Speleol. 37, 1–10.
Wu, D., Di, C., Wang, T., Wang, L., Chen, X., 2021. Characterization of the coherence between soil moisture and precipitation at regional scales. J. Geophys. Res.: Atmos. 126(8): e2020JD034340.
Wu, D., Wang, T., Di, C., Wang, L., Chen, X., 2020. Investigation of controls on the regional soil moisture spatiotemporal patterns across different climate zones. Sci. Total Environ. 726, 138214.
Xiang, W., Si, B.C., Biswas, A., Li, Z., 2019. Quantifying dual recharge mechanisms in deep unsaturated zone of Chinese Loess Plateau using stable isotopes. Geoderma 337, 773–781.
Xu, M., Liu, Q., Wu, D., Wang, T., Espoire, M., Chai, Q., 2022. Characterization of spatiotemporal patterns of soil water stable isotopes at an agricultural field. Sci. Total Environ. 828, 154538.
Yang, J., Chen, H., Nie, Y., Zhang, W., Wang, K., 2016. Spatial variability of shallow soil moisture and its stable isotope on a karst hillslope. Geoderma 264, 61–70.
Zhang, P., Shao, M., 2013. Temporal stability of surface soil moisture in a desert area of northwestern China. J. Hydrol. 505, 91–101.

Zhang, R., Xu, X., Liu, M., Zhang, Y., Xu, C., Yi, R., et al., 2018. Comparing evapotranspiration characteristics and environmental controls for three agroforestry ecosystems in a subtropical humid karst area. J. Hydrol. 563, 1042–1050.
Zhang, W., Wang, K., Chen, H., He, X., Zhang, J., 2012. Ancillary information improves kriging on soil organic carbon data for a typical karst peak cluster depression landscape. J. Sci. Food Agric. 92 (5), 1094–1102.
Zhang, Z., Chen, X., Cheng, Q., Soulsby, C., 2019. Storage dynamics, hydrological connectivity and flux ages in a karst catchment: conceptual modelling using stable isotopes. Hydrol. Earth Syst. Sci. 23 (1), 51–71.
Zhang, Z., Chen, X., Cheng, Q., Soulsby, C., 2021. Using StorAge Selection (SAS) functions to understand flow paths and age distributions in contrasting karst groundwater systems. J. Hydrol. 602, 126785.
Zhao, M., Gao, M., Chen, X., Zhang, Z., Li, M., 2015. Daily temperature characteristics and effect of spatial scale for different types of vegetation- a case study of Chenqi catchment in Guizhou Province. Resourc. Environ. Yangtze Basin 24, Z1. In Chinese.
Zhao, M., Hu, Y., Zeng, C., Liu, Z., Yang, R., Chen, B., 2018. Effects of land cover on variations in stable hydrogen and oxygen isotopes in karst groundwater: a comparative study of three karst catchments in Guizhou Province, Southwest China. J. Hydrol. 565, 374–385.
Zhao, Y., Peth, S., Wang, X.Y., Lin, H., Horn, R., 2010. Controls of surface soil moisture spatial patterns and their temporal stability in a semi-arid steppe. Hydrol. Process. 24 (18), 2507–2519.